One-pot synthesis of Ag-modified SrTiO3: synergistic effect of decoration and doping for highly efficient photocatalytic NOx degradation under LED

One-pot synthesis of Ag/$SrTiO_3$: synergistic effect of decoration and doping for highly efficient photocatalytic NO_x degradation under LED

Marcela Frias Ordoñez [a], Giuseppina Cerrato [b], Alessia Giordana [b], Alessandro Di Michele [c], Ermelinda Falletta[a,d*], and Claudia L. Bianchi [a,d].

a Department of Chemistry, University of Milan, Via Golgi 19, 20133 Milano, Italy

b Department of Chemistry, University of Turin, Via Pietro Giuria 7, 10125 Turin, Italy

c Department of Physics and Geology, University of Perugia, Via Pascoli 1, 06123 Perugia, Italy

d Consorzio Interuniversitario Nazionale per la Scienza e Tecnologia dei Materiali (INSTM), via Giusti 9, 50121 Florence, Italy

Corresponding author: ermelinda.falletta@unimi.it

Abstract

Strontium titanate is an ideal cubic-structure perovskite oxide that has shown great potential, especially within hydrogen production and water pollutants degradation field. However, its photocatalytic activity is limited under UV irradiation due to its wide energy band bap (~ 3.2 eV). In order to overcome this limitation, modification strategies such as metal-doping or metal-decoration have emerged. By applying these two approaches, a rational designing of 5 wt.% Ag-$SrTiO_3$ materials was performed for extending photocatalytic efficiency towards the degradation of NO_x under LED light. As a result, the Ag-decorated $SrTiO_3$ synthesized by wet-impregnation method photodegraded by nearly 77% within 3h under LED light. Whilst, through an eco-friendly, simpler, and valuable one-pot synthesis it was fabricated a highly efficient Ag-$SrTiO_3$ material that achieved complete photodegradation of NO_x, exhibiting a photoactivity 4 times higher than bare $SrTiO_3$. This new material was doubly modified by Ag^+ doping within the $SrTiO_3$ lattice and by Ag nanoparticles-decoration on the $SrTiO_3$ surface. The photocatalytic enhancement can be attributed to the synergetic

effect of Ag-doping and Ag-decoration on $SrTiO_3$, which contributed to a narrow band gap (2.80 eV), as well as the formation of heterojunctions that promotes the separation of photogenerated charges, respectively. The morphological, optical, structural, and physicochemical properties of the synthesized materials were fully investigated. The double modified photocatalysts showed good stability during recycling tests, maintaining high performances after three cycles. Eventually, active species were identified using various scavengers by trapping holes and radicals generated during the photocatalytic degradation process.

Keywords: One-step procedure; Ag-modified $SrTiO_3$ materials; NO_x photodegradation; Degradation mechanism

1. Introduction

Air pollution has become the front stage of global environmental issues since it threatens human health, the proliferation of diseases, and environmental disasters. The rapid growth of population, anthropogenic activities, and over-consumption of natural resources have been the leading causes of the increment of harmful pollutants levels over the last decades [1-3]. Some pollutants of significant public health concern include carbon monoxide, nitrogen oxides, sulfur oxides, ammonia, and volatile organic compounds (VOCs)[4]. Nitrogen oxides (NO_x) are primary pollutants directly linked to acid rains, photochemical smog, and respiratory problems. As a result, many countries and scientific communities have striven to mitigate and control NO_x emissions to the atmosphere by using several techniques, such as selective catalytic reduction (SCR) and non-selective catalytic reduction (NSCR), thermal and photocatalytic decomposition [5-7]. The latter is carried out at ambient conditions taking advantage of natural or artificial light in the presence of semiconductor materials. Therefore, photocatalysis is a green and cost-effective technology for the abatement of NO_x [4,8].

Perovskite oxides belong to the third generation of photocatalysts, which have been extensively explored for energy conversion and storage applications due to their unique properties[9]. Recently, their potential for environmental remediation, particularly organic and inorganic pollutants degradation, has been studied[10]. Among them, strontium titanate ($SrTiO_3$) stands out as a cubic-like structure perovskite with high thermal stability in comparison to TiO_2, which makes it attractive for its application on solar cells, gas sensors, and capacitors[11]. It is also a semiconductor with a wide energy band gap (3.2 eV), implying a high-efficiency photodegradation under UV irradiation [12]. However, UV

light is only 4% of the total solar spectrum [13]. Hence, as well as for TiO_2, modifying strategies for extending the photocatalytic performance within the visible region have been required, such as forming heterojunctions or incorporating defects into the lattice [14-15]. For instance, the design of a heterostructure between plasmonic nanoparticles (Ag, Au, or Pt) and $SrTiO_3$ (STO) surface has been studied by Chen et al. [16]. The authors reported the successful loading of Ag clusters (3-5 nm) over $SrTiO_3$ surface (~0.5 – 5 μm) via photoreduction method. Then, the fabricated Ag-$SrTiO_3$ composites (0.1 wt.%, 0.5wt.%, 1wt.%, 2wt.%, and 5wt.% Ag) were tested towards photocatalytic NO oxidation. The investigation determined 1%Ag-STO sample with the best photocatalytic performance, achieving 54% NO oxidation within 90 min under visible light irradiation. The improvement on the photocatalytic activity was attributed to the localized surface plasmonic resonance properties (LSPR) of Ag nanoparticles and the Schottky barrier formed at the interface of the metal and the semiconductor, promoting the separation of photogenerated charge carriers and prolonging their lifetime [17-18]. On the other hand, Zhang et al. synthesized the optimal 0.5% Ag-$SrTiO_3$ nanocomposite by one-pot solvothermal method. This composite was characterized by Ag spheres of 10-20 nm dispersed on the top of $SrTiO_3$ surface. However, the 0.5% Ag-$SrTiO_3$ material showed only a 30% of NO photocatalytic degradation under visible light within 30 min[19].

Taking into account these considerations, this work aimed to employ two synthetic approaches for the fabrication of Ag-$SrTiO_3$ materials and compared their photocatalytic efficiencies towards the NO_x abatement under LED light at ambient conditions. A conventional decoration procedure of the $SrTiO_3$ surface with pre-synthesized Ag nanoparticles (two-step process) and an innovative one-pot synthesis for both doping and decoration of $SrTiO_3$ were selected. The one-pot approach results very promising due to its economical, environmental and operational simplicity advantages. Moreover, the extreme conditions of heat treatment (900ºC) were chosen since Ag offers a high melting point nearby 961ºC and $SrTiO_3$ is characterized by high thermal stability[20-21]. Finally, the reusability of the most performing material has been adequately investigated, showing high stability for up to three runs, and active species were identified using various scavengers by trapping holes and radicals generated during the photocatalytic degradation process.

2. Materials and methods

2.1. Chemicals

Strontium acetate ($C_4H_6O_4Sr$), titanium (IV)isopropoxide ($C_{12}H_{28}O_4Ti$, 97%), silver nitrate ($AgNO_3$, ACS reagent, ≥99.0%), citric acid ($C_6H_8O_7$, ACS reagent, ≥99.5%), hydrogen peroxide (H_2O_2, 30%), KNO_3 (≥99.0%), polyvinylpyrrolidone (PVP), HNO_3 (ACS reagent, 70%), and acetone (ACS reagent, ≥99.0%) were purchased from Sigma Aldrich, Italia. All chemicals were used as received without further purification. An Ag^+ enriched solution was purchased from Argor-Heraeus SA (Mendrisio, Switzerland), the solution composition is described elsewhere [22].

2.2. Preparation of $SrTiO_3$ by a one-pot method

Strontium titanate (STO) was synthesized by a procedure previously described elsewhere [23]. First, a solution A was prepared by adding titanium (IV) isopropoxide (5.4 mmol) dropwise into deionized water (20 mL) under vigorously stirring. Then, citric acid (10.8 mmol) was added to the previous suspension in a 2/1 molar ratio with respect to Ti-ions. Afterwards, hydrogen peroxide 30% (2.6 mL) was added until the complete dissolution of titanium hydroxide formed an orange-colored solution [24]. A solution B was obtained by dissolving a stoichiometric amount of strontium acetate (5.4 mmol) in a minimum amount of deionized water (7 mL). Then, citric acid (10.8 mmol) was added in a molar ratio 2/1 with respect to Sr^{2+} ions. Both solutions were mixed at room temperature under vigorous stirring for 3 hours. Subsequently, the solution was heated at 70ºC. Before complete evaporation, the orange solution was transferred into a crucible and dried at 75ºC for 12ºh and at 120ºC for 12 h. The sample was calcined at 900ºC adopting the following ramp (0.5ºC/min from 25 to 250ºC, time 1 min; 2.5ºC/min from 250 to 900ºC, time 60 min).

This material was used as it is and for the preparation of Ag-decorated $SrTiO_3$, as described below (section 2.4.).

2.3. Preparation of Ag-$SrTiO_3$ (Ag/STO) by one-pot approach

Ag-$SrTiO_3$ materials were synthesized by the one-pot method described above [23] with the difference that the solution B was obtained by dissolving silver ions (0.5 mmol) and strontium acetate (4.9 mmol) in a minimum amount of deionized water (7 mL). Then, citric acid (10.8 mmol) was added in a molar ratio 2/1 with respect to the sum of ions of

98 Ag^{+} and Sr^{2+} ions. Both solutions were mixed at room temperature under vigorous stirring for 3 hours. Subsequently,
99 the solution was heated at 70ºC. Before complete evaporation, the orange solution was transferred into a crucible and
100 dried at 75ºC for 12ºh and at 120ºC for 12 h. The samples were calcined at 900ºC adopting the following ramp (0.5ºC/min
101 from 25 to 250ºC, time 1 min; 2.5ºC/min from 250 to 900ºC, time 60 min).

102 Depending on the Ag source, the final materials were labeled Ag/STO1 (from the Ag^{+} enriched solution) and Ag/STO2
103 (from pure $AgNO_3$ from Sigma Aldrich).

104 *2.4. Preparation of Ag-decorated $SrTiO_3$ (Ag@STO) by multistep approach*

105 Ag nanoparticles (5 wt.%) were deposited onto STO surface (Ag@STO) via a wet impregnation method on the basis of
106 the literature [22]. The STO (44 mmol) synthesized as described above (section 2.2.) was dispersed in 10 mL acetone.
107 Then, 13 mL of a 30 g/L solution of Ag nanoparticles, previously synthesized by an electrochemical method starting
108 from the silver-enriched wastewater source, were added [22, 25]. The mixture was stirred at 40ºC for 24h. Afterwards,
109 the temperature was raised up to 120ºC under stirring for 1 h in order to evaporate the solvent. The remained product
110 was dried overnight at 100ºC and further calcined at 900ºC adopting the following ramp: 300ºC for 2h, 600ºC for 1h,
111 and 900ºC for 1h (9ºC/min).

112 *2.5. Materials characterization*

113 The crystal structure and phase composition of the synthesized samples were determined by X-ray diffraction (XRD)
114 employing a Rigaku-Miniflex-600 diffractometer using Cu-Kα radiation (λ= 1.541874 Ă). All the diffractograms were
115 collected between 10º - 80º (2θ) at 3º min^{-1} with a step of 0.02º (2θ). The calculation of the crystallize size of the pure
116 and Ag-modified $SrTiO_3$ materials was estimated by the Scherrer equation (Eq. 1) using the peak at 46.4º that
117 corresponds to 200 reflection plane, where D is the crystallite size, k is the shape factor, λ is the X-ray wavelength of
118 radiation for Cu(kα), β_{hkl} is the full-width at half maximum (FWHM) at (hkl) peak, and θ_{hkl} is the diffraction angle.

119 $$D = \frac{k\lambda}{\beta_{hkl} Cos\theta_{hkl}} \quad \text{(Eq. 1)}$$

120 Specific surface area (SSA) and porosity (pore volume) were determined by N_2 adsorption/desorption isotherms
121 collected at -196ºC on a Micrometrics Tristar II 3020 (Micromeritics) with Brunauer-Emmett-Teller (BET) equation (two

parameters, $0.05 < p/p_0 < 0.3$). Before the analysis, the sample was treated at 150ºC for 4h under vacuum-adsorbed foreign species. UV-Vis diffuse reflectance spectra were carried out at room temperature on a Perkin Elmer Lambda 35 UV-Vis Spectrometer equipped with an integrating sphere. The data were converted using the Kubelka-Munk formula. X-ray photoelectron spectroscopy (XPS) measurements were performed on a M-probe apparatus equipped with an Al Kα source (hv= 1486.6 eV). Survey scans were measured between 0-1100 eV binding energy range with 5 eV energy resolution. The morphology and composition of the samples were evaluated by field emission gun electron scanning microscopy (FE-SEM, model LEO 1525 Zeiss), coupled with a Bruker Quantax EDX. The acceleration potential voltage was maintained at 15 keV and measurements were carried out using AsB detector (Angle selective Backscattered detector) and In-lens detector. The HRTEM images were collected using a JEOL 3010-UHR instrument (acceleration potential: 300 kV; LaB6 filament).

2.6 Photocatalytic tests

The sample was prepared by suspending 50 mg of each photocatalyst in 5 mL isopropanol. An ultrasonic bath was used to sonicate the suspension in order to obtain a uniform dispersion. Then, a thin film was deposited on a glass plate (3.3 cm x 11.5 cm) by drop casting. After the solvent was evaporated, the glass plate with the photocatalyst was placed inside a 20L Pyrex reactor. The reactor was filled in with NO_x gas at the initial concentration of 500 ± 50 ppb (by feeding 0.625% of NO_2 and 0.125% of NO, diluted with air). The tests were carried out at room temperature for 3 hours under LED irradiation (350 mA, 9-48V, 16.8W), yielding an intensity of 2900 lx on the photocatalyst surface. An ENVEA AC32e chemiluminescence detector directly connected to the reactor measured the NO_x concentration at 30, 60, and 180 min. Photolysis tests indicate 10% of pollutant degradation after 3h of light irradiation. Lastly, the most performing photocatalyst (Ag/STO2) was subjected to recycling tests (three tests under the same experimental conditions without any post-treatment) in order to assess the stability.

2.7 Scavenging experiments

In order to investigate the reaction pathway, the photocatalytic tests were carried out in the presence of scavenger agents using the procedure reported in the literature [26,28]. Potassium iodide (KI), potassium dichromate ($K_2Cr_2O_7$),

tert-butyl alcohol (TBA) and p-benzoquinone (PBQ) were employed as scavengers for h^+, e^-, $^{\bullet}OH$ and $O_2^{\bullet-}$, respectively. Briefly, the photocatalyst (50 mg) was mixed with the proper radical scavenger (1 mmol) in deionized water (10 mL) and ultrasonicated for 15 min. Afterwards, the suspensions were deposited onto glass plates, followed by a drying process at 60ºC until the water was completely evaporated. The plates were used to test the photocatalytic degradation of NO_x under LED light, as described above.

3 Results and discussion

In order to investigate the effect of Ag-modification on STO, all the synthesized materials were extensively characterized by several techniques, as described below.

3.1 Photocatalysts characterization

The crystal structures of the synthesized materials were analyzed using X-ray diffraction (XRD) and the obtained results are showed in Figure 1.

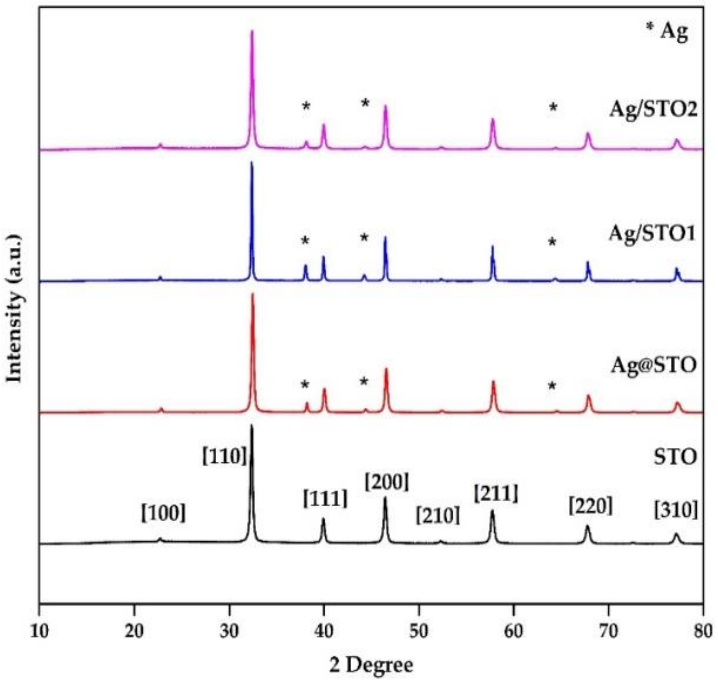

Figure 1. XRD patterns of prepared samples.

The XRD data (Figure 1) evidenced the presence of peaks located at 22.7º, 32.4º, 39.9º, 46.4º, 52.3º, 57.7º, 67.7º, and 77.1º, which are identified as (100), (110), (111), (200), (210), (211), (220), (310) planes of a cubic perovskite structure (space group: P3m3) of strontium titanate. Compared to pristine STO, the samples Ag@STO, Ag/STO1, and Ag/STO2 exhibited

169 additional diffraction peaks located at around 38º, 44º and 64º, corresponding to metallic Ag on the surface of strontium
170 titanate. More in detail, they can be indexed to the (111), (200) and (220) planes of cubic Ag phase. The average
171 crystallite sizes were about 51 nm, 61 nm, 108 nm, and 54 nm for STO, Ag@STO, Ag/STO1 and Ag/STO2, respectively,
172 as estimated from the half-peak width of the (200) diffraction peak (Table 1). It can be observed that the particle size
173 was no dramatically affected by the synthesis procedure. However, the Ag/STO1 demonstrated a slight growth of the
174 particle size. This could be associated to the presence of large amount of impurities (i.e. Cu, Fe, As, Ni, Pb, Zn) in the
175 sample coming from the Ag^{+} enriched wastewater. In contrast with the scientific literature, from the XRD patterns of
176 the three modified photocatalysts (Ag@STO, Ag/STO1 and Ag/STO2) is difficult to distinguish the characteristic shift
177 associated to the introduction of a dopant into the host lattice ($SrTiO_3$), because all the diffractograms, also that of
178 Ag@STO, exhibited a slight shift towards the higher angles.

179 **Table 1.** Average crystallite size, specific surface area (SSA), pore size, bandgap energy, rate constants of the
180 prepared photocatalysts.

Photocatalyst	Average crystallite size (nm)	SSA (m^2/g)	Pore Size (nm)	Energy Bang (eV)	Rate Constant (min^{-1})
STO	51	16	33	3.2	0.002
Ag @STO	61	13	32	3.1	0.009
Ag/STO1	108	2	9	3.0	0.002
Ag/STO2	54	15	19	2.8	0.018

181

182

Since the photocatalytic performance is strongly linked to the surface properties of the material [29], the surface area of all the photocatalysts was properly investigated (Figure 2 and Figure S1). According to the IUPAC classification, all the materials exhibited isotherms type IV, characteristic of mesoporous materials [29]. The specific surface areas (SSA) of all the samples are presented in Table 1. Among the Ag-$SrTiO_3$ samples, the Ag/STO2 photocatalyst showed the biggest BET surface area (15 m^2g^{-1}), which is beneficial for better adsorption of nitrogen oxide molecules and provides a more significant number of reactive sites for enhancing photocatalytic activity [30-31]. On the other hand, the Ag/STO1 sample exhibited the lowest BET surface area, suggesting that also in this case the large amount of impurities present in the Ag-enriched wastewater might adversely affect the properties of the material. Moreover, this is in accordance with the XRD results, showing very large crystallite size for this material. Lastly, the Ag@STO sample showed a slight reduction in BET surface area (13 m^2g^{-1}), which should be ascribed to a double calcination treatment that the material was undergone[32-33].

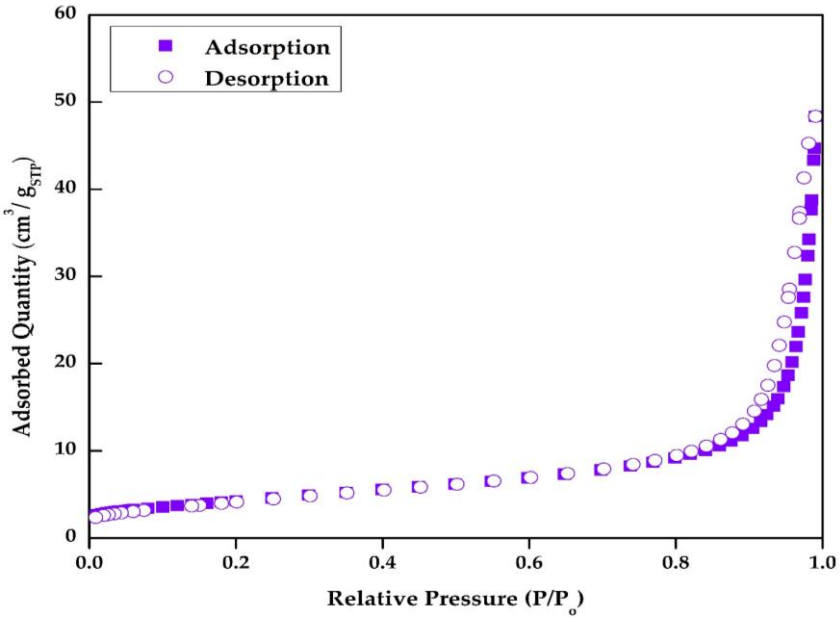

Figure 2. Nitrogen adsorption-desorption isotherm for Ag/STO2

The optical properties of the as-prepared samples were investigated by UV-Diffuse Reflectance Spectroscopy (UV-DRS). The data were collected between 200-700 nm and transformed into absorption spectra by applying the Kubelka-Munk function (Figure 3a) [34-35]. As a result, STO photocatalyst showed a wide energy band gap (Table 1), typical of pristine $SrTiO_3$ that possesses the absorption edge in the UV light region (Figure 3b)[36-38]. After its surface decoration

with Ag nanoparticles (NPs), Ag@STO photocatalyst exhibits a higher light absorption within the visible region characteristic of the localized surface plasmon resonance (LSPR) effect. The latter suggests the promotion of electron-hole pair separation and hence a higher photocatalytic activity. Interestingly, by changing the synthetic procedure to one-step process the energy band gap and the absorbance got definitely modified. The Ag/STO1 and Ag/STO2 displayed a nominal band gap of 3.0 and 2.8 eV, respectively. In particular, Ag/STO2 showed at the same time a greater absorbance in the visible region which, in accordance to the presence of Ag clusters, and low value of energy band gap, are highly beneficial for photocatalytic properties, exploiting the synergistic effect of both decoration and doping. Lastly, it has to be highlighted that the source of Ag might have negatively affected the response of the final Ag-$SrTiO_3$ material, since there was no significant variation in the energy band gap.

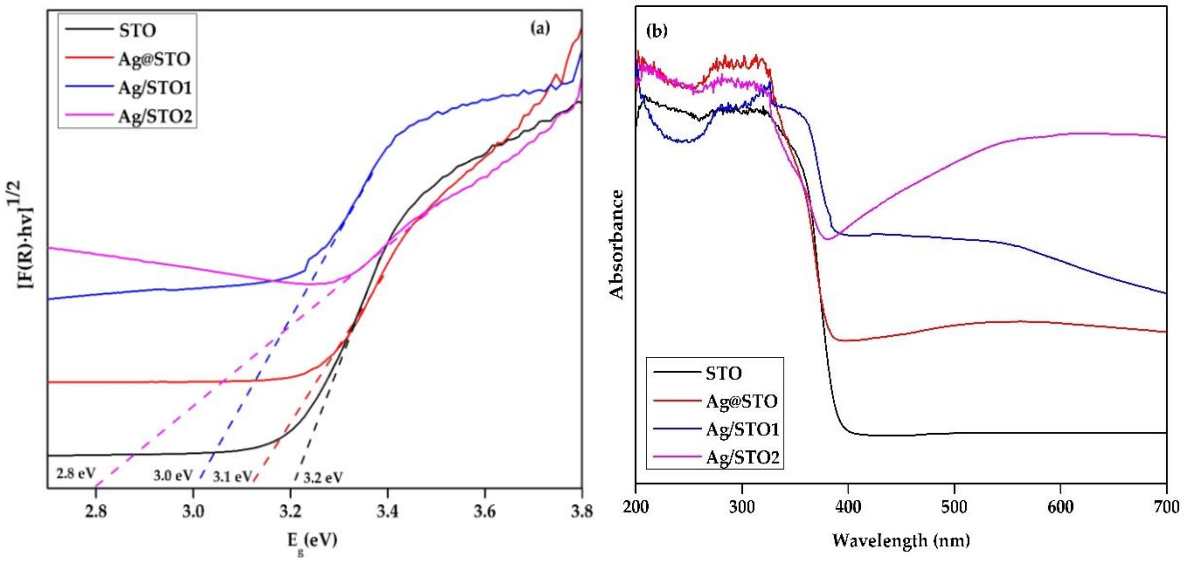

Figure 3. (a) Tauc plots and (b) UV-Visible diffuse reflectance spectra of bare STO and Ag- $SrTiO_3$ samples.

As it will be discussed below, Ag/STO2 resulted to be the most performing photocatalyst, therefore, this material was characterized more in depth.

To investigate the morphological features of Ag/STO2, SEM and HRTEM analyses were performed (Figure 4). From Figure 4a, it can be seen aggregated $SrTiO_3$ particles with not well-defined shape, and their size is in the 40-70 nm range. The further HRTEM analysis was resorted to, in order to investigate the possible presence of Ag NPs, to confirm the average size of STO particles and in some extent the general morphology as well. All the small nanoparticles can be referred to Ag species on the basis of the EDX analysis (see the Figure S2), confirming the indications coming from XRD investigations.

The Ag species were uniformly distributed onto the $SrTiO_3$ surface and exhibited a roundish morphology with an average size of 2 nm. Their metallic character was also confirmed by the FFT calculations of the fringes (see the inset to Figure 4c), in which the (1 1 1) family of metallic Ag is evidenced (ICDD file No. 004-0783). Moreover, the HRTEM results provided evidence that $SrTiO_3$ particles displayed a cubic morphology. The amounts of Sr, Ti, Ag, and O elements were confirmed being in the ratio expected from the theoretical stoichiometry. The Ag element was homogeneous dispersed on $SrTiO_3$ and it was found in an atomic ratio of 0.09 respect to Sr. An excess of oxygen on the Ag/STO2 surface was observed, which can be explained by calcination treatment at 900°C in air.

Hence, bearing in mind these results and the UV-DRS experimental data, it can be implied that an amount of Ag would be successfully introduced into $SrTiO_3$ lattice, responsible of the energy band gap modification, whereas the excess of Ag would remain as metallic silver on $SrTiO_3$ surface, as demonstrated by the morphological characterization. This synergistic effect of Ag-doping and Ag decoration will positively impact the photo response of Ag/STO2.

Lastly, in order to compare the results obtained for Ag/STO2 with those of Ag@STO, the latter was investigated by FE-SEM. In Figure S3, roundish micro-sized particles (0.5 – 1.5 μm average size) were deposited on STO surface. It is clear that these are Ag particles with a much larger dimension than those observed on Ag/STO2 (less than 2 nm). Therefore, by using a conventional decoration process (two-step), the Ag particles deposited onto $SrTiO_3$ surface exhibit these features, that might negatively impact the surface area of the composite material and further limited its photocatalytic performance[39].

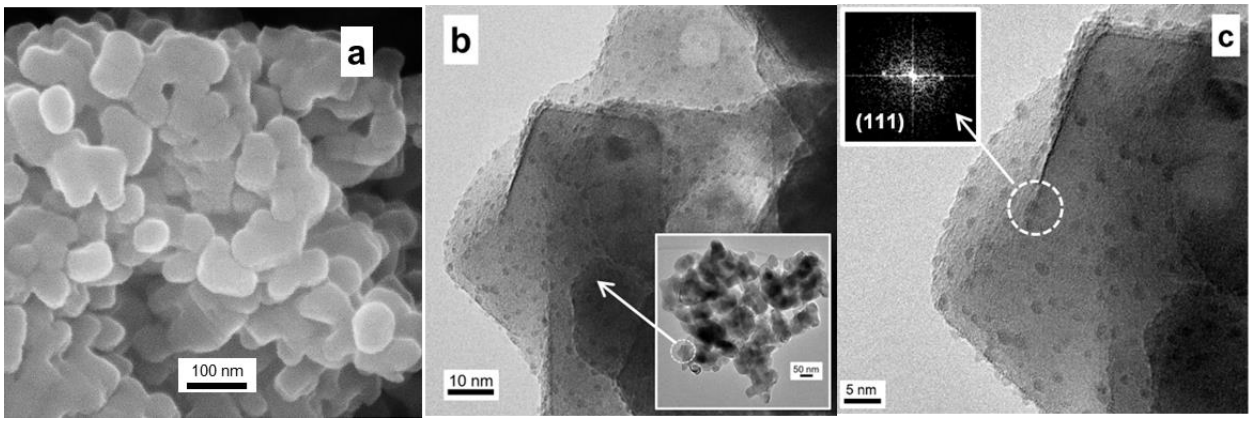

Figure 4. (a) SEM image of Ag/STO2 and (b,c) TEM-HR-TEM images of Ag/STO2: the inset to Figure 4b represents a low magnification overview, whereas the inset to Figure 4c refers to the FFT (simulating the electron diffraction) of the evidenced nanoparticle.

To identify the surface chemical states of the Ag/STO2 photocatalyst, XPS analysis was performed[40]. The survey spectrum (Figure S4) reports the typical photopeaks associated with Sr 3d (133.1 eV), Ti 2p (464.6 eV), O 1s (529.8 eV), Ag 3d (368.0 eV), and C 1s (284.6 eV), the latter was ascribed to adventitious carbon during XPS measurement. The C 1s photopeaks are composed of three components (C-C, C-O, and C=O) with respective binding energies 284.6, 286.1, and 287.5 eV (Figure S5)[41]. The high resolution (HR) Sr 3d spectrum (Figure 5a) showed the formation of a doublet signal at 133.1 and 134.8 eV, associated with Sr $3d_{5/2}$ and Sr $3d_{3/2}$, respectively. These values are in good agreement with the reported values in the literature for the Sr^{2+} state in $SrTiO_3$ with a 1.7 eV splitting [42-43]. Regarding Ti, the two main peaks of Ti $2p_{3/2}$ and Ti $2p_{1/2}$ centered at 458.7 and 464.6 eV, respectively, and a doublet splitting of 5.8 eV, verify the existence of Ti^{4+} [42,44]. In Figure 5c, the characteristic binding energies of Ag $3d_{5/2}$ and Ag $3d_{3/2}$ of metallic silver are at 368.0 and 374.0 eV for [45], whereas 3d Ag sub-peaks located at 368.9 and 374.9 eV were attributed to the presence of silver ion, usually assigned to Ag_2O state [46]. Lastly, the O1s high-resolution region was described by two peaks at 529.0 and 531.7 eV, corresponding to lattice oxygen and hydroxyl groups, respectively [47-48].

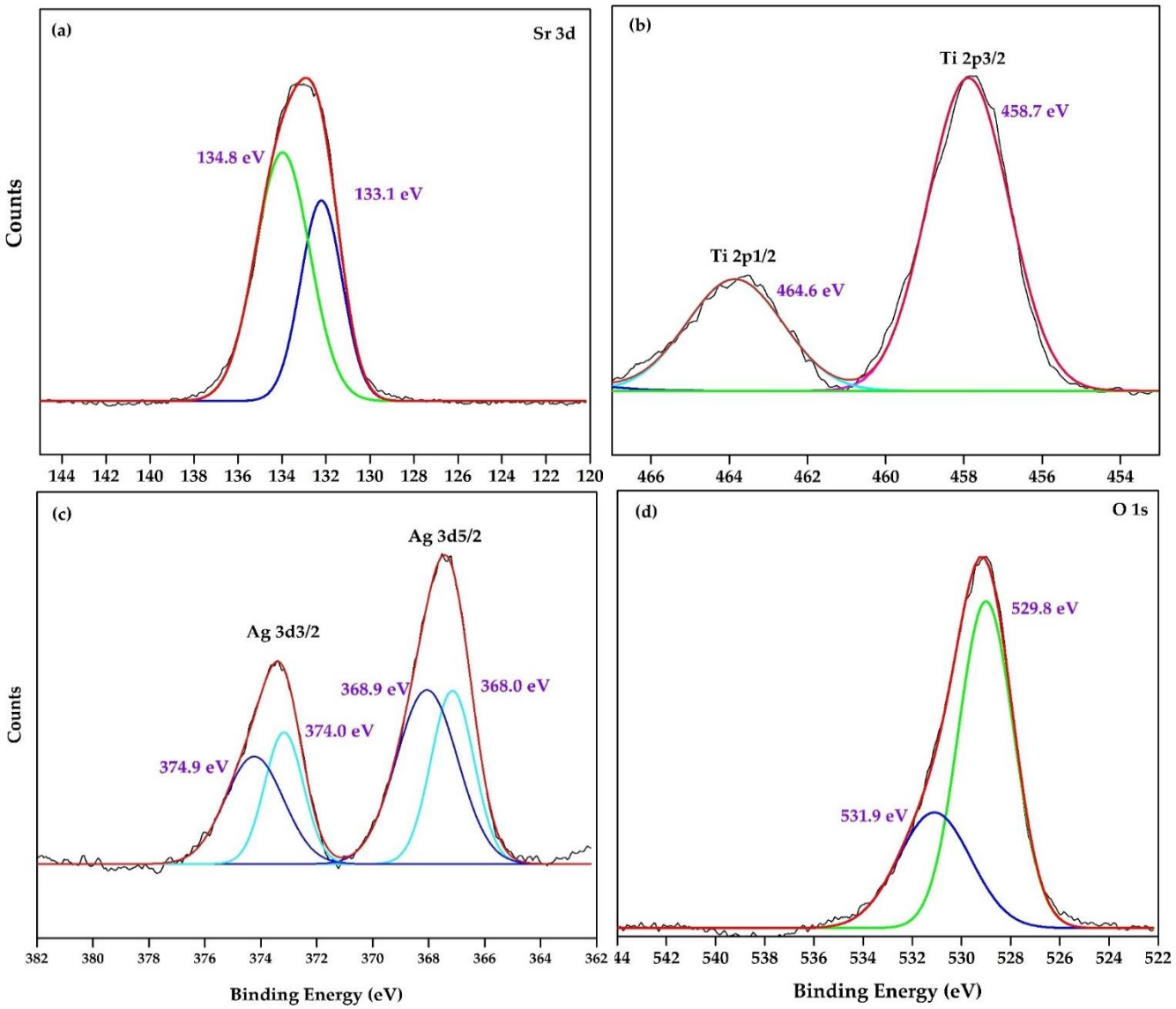

Figure 5. XPS HR spectra of (a) Sr 3d, (b) Ti 2p, (c) Ag 3d and (d) O 1s of Ag/STO2 photocatalyst.

3.2 *Photocatalytic activity*

The photocatalytic activity of the synthesized samples was tested towards the degradation of NO_x under LED light (400-700 nm) for 3 hours. For comparison, the photolysis of nitrogen oxide gases in the absence of any photocatalysts was investigated under the same experimental conditions. The results suggest that photolysis was negligible on the degradation process (Figure S6).

The photodegradation rates of nitrogen oxides as a function of the irradiation time over all the photocatalysts are plotted in Figure 6a. As expected, pristine STO sample was inactive under LED light due to their large energy bandgap

(3.2 eV)[49-50]. The STO surface's modification by Ag nanoparticles decoration (Ag@STO) leads to a significant increase of the photocatalytic efficiency, achieving nearly 77% of NO_x photocatalytic abatement under LED light within 3 hours. The enhancement was ascribed to the localized surface plasmon resonance (LSPR) effect that boosted the photoinduced charge separation, despite the micrometric – sized of the Ag nanoparticles. Nonetheless, the small specific surface area due to a double calcination treatment at 900C, and a large band energy value might have adversely inhibited the fully photocatalytic degradation of nitrogen oxides under LED light after 180 min [22,29].

On the other hand, the performances of the materials synthesized by the one-pot procedure seem to be strongly correlated to the purity of the Ag source. In fact, for Ag/STO1 and Ag/STO2 two different outcomes were obtained. The Ag/STO1 photocatalyst showed a photocatalytic efficiency similar to bare STO. This result suggests that the large amount of impurities present in the Ag^+ enriched wastewater might play a deactivating role on the photocatalyst. On the other hand, the Ag/STO2 photocatalyst synthesized with pure Ag demonstrated an extraordinary photocatalytic efficiency greater than that obtained by Ag@STO. In fact, after 3 hours of LED irradiation, Ag/STO2 is capable to completely degrade nitrogen oxides. This photocatalyst revealed a larger specific surface area (16 m^2g^{-1}) in comparison to Ag/STO1 [51-53]. Most importantly, it is evidenced the synergic effect of Ag^+-doping and Ag-decoration, which is noticed in a reduction in the band gap (2.80 eV) and the presence of small Ag clusters (average size 2 nm) that boosted up the separation of charge carriers through LSPR effect [16,54]. The photocatalytic efficiency of Ag/STO2 was 4 times greater than bare STO.

The corresponding first-order kinetics plot is shown in Figure 6b. It indicates that Ag/STO2 photocatalyst exhibited the highest degradation rate (0.018 min^{-1}), which is almost 9 times greater than the bare $SrTiO_3$ and Ag/STO1 prepared in similar experimental conditions (0.002 min^{-1}). Conversely, concerning the Ag-decorated photocatalyst (Ag@STO), the rate (0.009 min^{-1}) is five times faster than bare STO, and it is two times slower than Ag/STO2. These results suggest that the photocatalytic performance of the final Ag-$SrTiO_3$ materials is totally impacted by the synthesis method and the source of Ag used. Nevertheless, one-pot solution synthesis carried out in the presence of pure Ag source stands out as an attractive, feasible, one-step alternative for the fabrication of double-modified Ag-$SrTiO_3$ materials (Ag^+-doped and Ag-decorated) with extraordinary physicochemical, morphological, optical, and photocatalytic properties.

293 Lastly, the stability of the Ag/STO2 nanostructure was further evaluated by reusing the photocatalyst for degrading
294 NO_x gases under LED light. Three successive photocatalytic experimental runs were carried out under similar
295 experimental conditions. As shown in Figure 6c, the efficiency decreased by 5% only, demonstrating no significant loss
296 after three repeated runs. Therefore, the Ag/STO2 photocatalyst is a stable material for prolonged usage and practical
297 application for the photocatalytic degradation of NO_x under LED light.
298
299
300

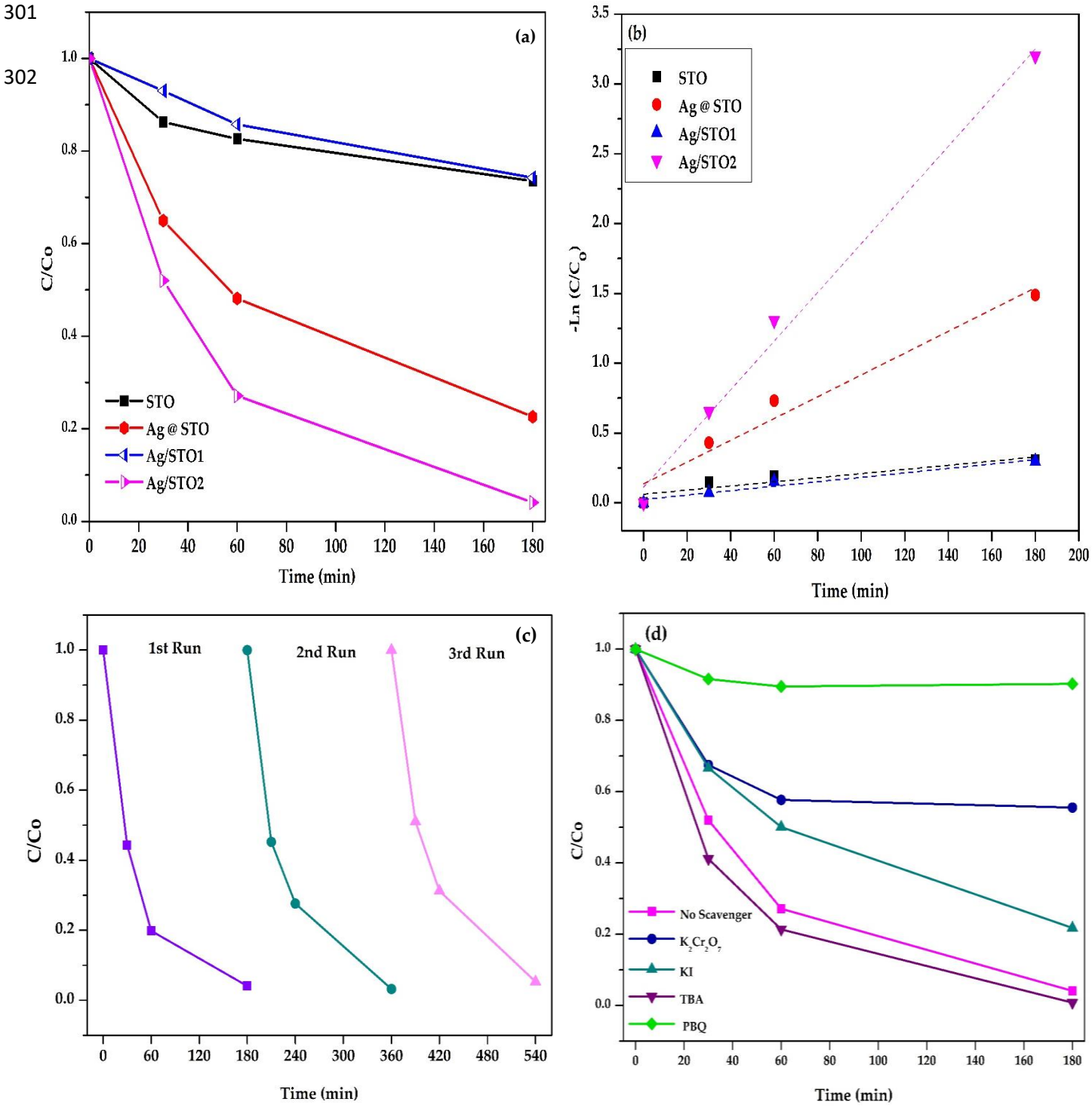

Figure 6. (a) NO_x photocatalytic removal efficiency C/Co as a function of time and (b) First-order kinetic plot of synthesized STO, Ag@STO, Ag/STO1, and Ag/STO2 materials; (c)reusability of Ag/STO2 photocatalyst for the NO_x degradation under LED irradiation; (d) NO_x photocatalytic removal efficiency under LED irradiation with the addition of potassium dichromate, potassium iodide, tert-butanol (TBA) and p-Benzoquinone as electrons, holes, •OH radicals and $\bullet O_2^-$ scavengers, respectively.

3.3 *Mechanism of NO_x photodegradation*

In order to explore the reaction mechanism of NO_x photodegradation, the scavenger tests were performed in order to determine the active species mainly responsible for the degradation of nitrogen oxides under LED light. During the photocatalytic process, the photogenerated holes (h^+) and electrons (e^-) can drive the redox reactions directly. However, they can also trigger the production of other oxidizing species, such as hydroxyl radicals ($^{\bullet}OH$) and superoxide anion radicals ($O_2^{\bullet-}$), which indirectly start the degradation process of NO_x [5]. Potassium iodide, potassium dichromate, *tert*-butyl alcohol (TBA), and p-benzoquinone (PBQ) were added to capture holes, electrons, $^{\bullet}OH$ and $O_2^{\bullet-}$ radicals, respectively[27,55,56]. As can be seen in Figure 6d, by the addition of TBA, the photocatalytic efficiency of Ag/STO2 demonstrated similar performance as in the absence of the scavenger. In contrast, the addition of PBQ thoroughly depressed the photoactivity, which indicates that $O_2^{\bullet-}$ has a crucial role during the NO_x removal process. It is also clear that the photodegradation of NO_x was also reduced by the addition of KI and $K_2Cr_2O_7$, showing a significant inhibition but not a complete quenching of the reaction. These results confirm that photogenerated h^+, e^- and $O_2^{\bullet-}$ play a key role in photocatalytic NO_x degradation under LED light.

Similarly, the band edge positions of the photocatalysts are very important for the generation of active species during the photocatalytic process. From the band gap shown in the Figure 3a and Table 1, it is possible to calculate the positions of the minimum conduction band edge (CB) and maximum valence band edge (VB) of STO with respect to a normal hydrogen electrode (NHE), according to the following equations:

$$E_{CB} = X - E_e - \frac{1}{2}E_g \quad \text{(Eq. 2)}$$

$$E_{VB} = E_{CB} + E_g \quad \text{(Eq. 3)}$$

X is the absolute electronegativity of the semiconductor, which can be calculated as the geometric mean of the absolute electronegativity of the constituent elements of the semiconductor [57]. The E_g is the band gap energy of the semiconductor, and E_e is the energy of the free electrons on the hydrogen scale (~ 4.5 eV). The electronegativity of Ag-modified $SrTiO_3$ (X) was estimated to be 5.36 eV [58]. Therefore, the E_{CB} and E_{VB} for Ag/STO2 were estimated to be -0.58 eV and 2.22 eV, respectively. These results indicate that the conduction band of Ag/STO2 is negative compared to the reduction potential of $O_2/O_2^{\bullet-}$ (-0.33 eV). This suggests that it is easier for the photogenerated electrons to react with

O_2 to form $O_2^{\bullet-}$ placed in the conduction band of Ag/STO2. Correspondingly, the valence band of Ag/STO2 is positive compared to the redox potential for $OH^{\bullet}$ ($OH^-/OH^{\bullet}$) at 1.99 eV, indicating that the formation of $OH^{\bullet}$ by the holes of $SrTiO_3$ is feasible [59-60]. The previous results are in line with the findings observed during the trapping experiments. The proposal reaction pathway is summarized in Figure 7.

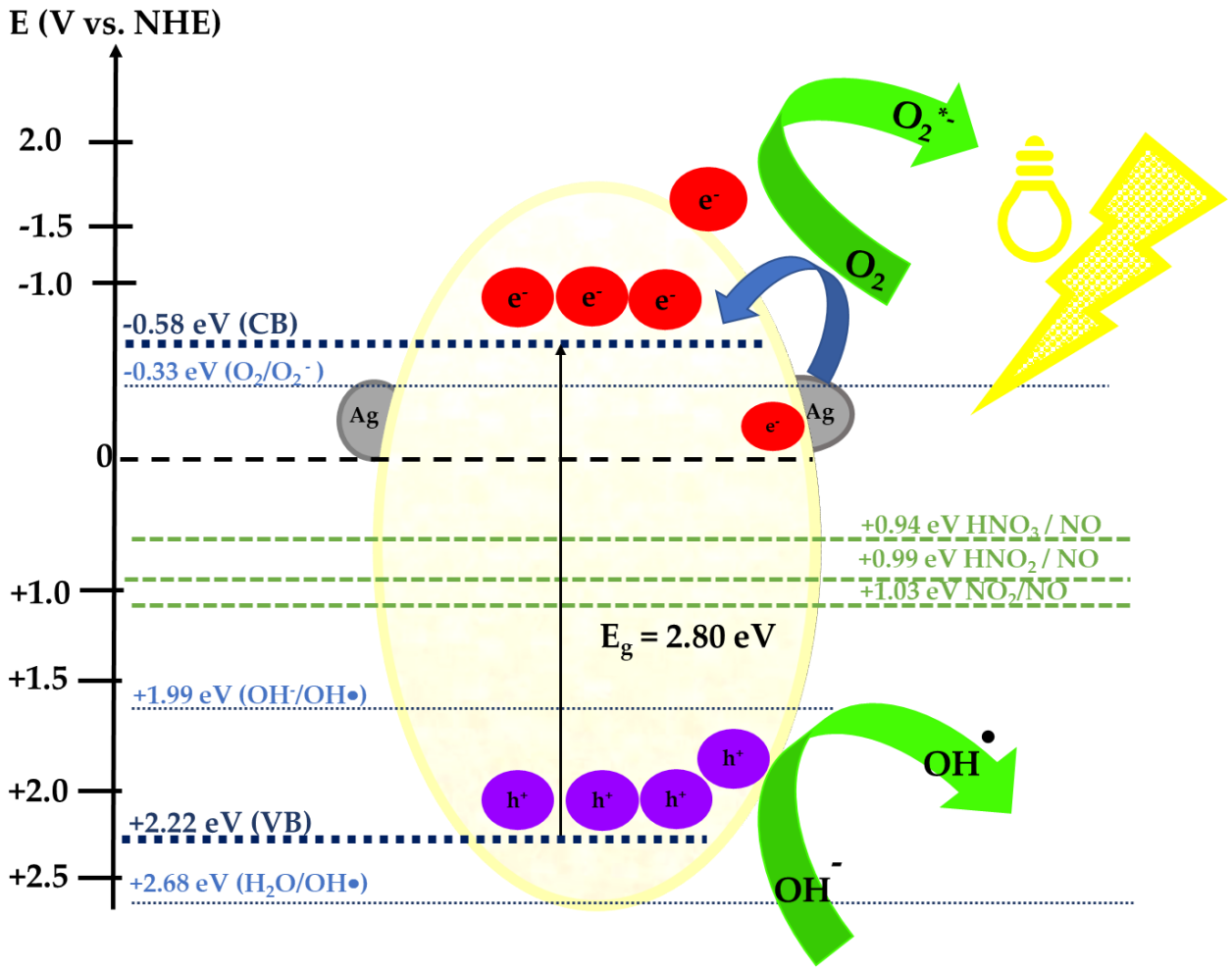

Figure 7. Scheme of photocatalytic degradation of NOx under LED light.

When the Ag/STO2 photocatalyst is excited by LED light at the plasmonic frequency of Ag clusters, photoelectrons are produced and transferred to the conduction band of $SrTiO_3$ by overcoming the Schottky barrier at the metal/semiconductor interface (Eq. 4-5). Then, the hot electrons react with the adsorbed oxygen to produce superoxide anion and hydroxyl radicals (Eq. 6-8). The introduction of Ag into the $SrTiO_3$ lattice is reflected by the rise of the valence band with respect to the original $SrTiO_3$. The electrons present in the valence band can migrate to the E_f (fermi level) of

Ag nanoparticles, leaving behind holes that can react with hydroxyl groups to produce hydroxyl radicals (Eq. 9). Lastly, the O_2^- and •OH radicals control the NO_x degradation process (Eq. 10-12)[19,27].

$$Ag_{clusters} + \lambda_{visible} \rightarrow Ag_{clusters}^{*} \quad \text{(Eq. 4)}$$

$$Ag_{clusters}^{*} + SrTiO_3 \rightarrow SrTiO_3(e_{CB}^-) \quad \text{(Eq. 5)}$$

$$SrTiO_3(e_{CB}^-) + O_2 \rightarrow {}^{\bullet}O_2^- \quad \text{(Eq. 6)}$$

$${}^{\bullet}O_2^- + 2H^+ + SrTiO_3(e_{CB}^-) \rightarrow H_2O_2 \quad \text{(Eq. 7)}$$

$$H_2O_2 + SrTiO_3(e_{CB}^-) \rightarrow {}^{\bullet}OH + OH^- \quad \text{(Eq. 8)}$$

$$SrTiO_3(h_{VB}^+) + OH^- \rightarrow {}^{\bullet}OH \quad \text{(Eq. 9)}$$

$$NO + {}^{\bullet}OH \rightarrow HNO_2 \quad \text{(Eq. 10)}$$

$$NO_2 + {}^{\bullet}OH \rightarrow NO_3^- + H^+ \quad \textit{(Eq. 11)}$$

$$NO + {}^{\bullet}O_2^- \rightarrow NO_3^- \quad \text{(Eq. 12)}$$

Conclusions

In this work, $SrTiO_3$ has been successfully modified using two strategies to extend its photocatalytic efficiency in the degradation of NO_x under LED light: decoration by a two-steps approach, and doping and decoration by a one-step method. By the two-step process, the $SrTiO_3$ surface was loaded with pre-synthesized Ag nanoparticles starting from an Ag-enriched wastewater. The heterostructure material achieved nearly 77% NO_x removal after 3h under LED light.

Whilst, the one-pot process demonstrated to be a prominent method for the fabrication of an outstanding doubly Ag-modified $SrTiO_3$ photocatalyst (Ag^+ - doping and Ag-decorated). However, when the reaction was carried out by the Ag^+-enriched wastewater, the presence of large amount of impurities completely nullified the effect of the Ag, whereas the photocatalyst prepared by a pure Ag source (Ag/STO2) showed excellent activity. Ag/STO2 photocatalyst exhibited a narrow band gap and Ag metallic nanoparticles (size 2 nm) loaded on STO surface, besides a large specific surface area (16 m^2g^{-1}). The synergistic effect between Ag^+-doping and Ag-decorated had essentially contributed to the thorough NO_x photodegradation within 3h under LED light. Therefore, a one-pot synthesis is an eco-friendly, simpler, and valuable process for the design of Ag-$SrTiO_3$ materials with double modification (within the $SrTiO_3$ lattice and $SrTiO_3$ surface) that allows the extension and enhancement of photocatalytic efficiencies of $SrTiO_3$ towards NO_x abatement under LED light.

Finally, the Ag/STO2 photocatalyst showed good photocatalytic activity without significant loss over the degradation efficiencies of NO_x after three consecutive runs. Concerning the degradation mechanism, trapping experiments confirmed that the photogenerated h^+, e^- and $O_2^{\bullet-}$ species are the major reactive species responsible for NO_x photodegradation in the Ag/STO2 surface.

CRediT authorship contribution statement

Marcela Frias Ordoñez: Methodology, Formal analysis, Investigation, Data Curation, Writing-Original Draft. **Giuseppina Cerrato:** Formal analysis, Data curation, Writing- Review & Editing. **Alessia Giordana:** Formal analysis, Data curation**. Alessandro Di Michele:** Formal analysis, Data curation. **Ermelinda Falletta:** Conceptualization, Methodology, Data Curation, Validation, Supervision, Writing - Review & Editing, **Claudia L. Bianchi:** Conceptualization, Data Curation, Supervision, Writing - Review & Editing, Project administration, Funding acquisition.

Data availability

Data will be made available on request.

Declaration of competing interest

The authors declare that they have no known competing financial interests or personal relationships that could have appeared to influence the work reported in this paper.

Acknowledgements

The authors thank Carolina Peverelli for materials preparations and photodegradation tests.

Appendix A. Supplementary data

References

[1] K. W. Tham, "Indoor air quality and its effects on humans—A review of challenges and developments in the last 30 years," *Energy Build.*, vol. 130, pp. 637–650, 2016, doi: 10.1016/j.enbuild.2016.08.071.

[2] F. J. Kelly and J. C. Fussell, "Air pollution and public health: emerging hazards and improved understanding of risk," *Environ. Geochem. Health*, vol. 37, no. 4, pp. 631–649, 2015, doi: 10.1007/s10653-015-9720-1.

[3] I. Khan, F. Hou, and H. P. Le, "The impact of natural resources, energy consumption, and population growth on environmental quality: Fresh evidence from the United States of America," *Sci. Total Environ.*, vol. 754, p. 142222, 2021, doi: 10.1016/j.scitotenv.2020.142222.

[4] A. K. Priya, R. Suresh, P. S. Kumar, S. Rajendran, D. V. N. Vo, and M. Soto-Moscoso, "A review on recent advancements in photocatalytic remediation for harmful inorganic and organic gases," *Chemosphere*, vol. 284, no. May, p. 131344, 2021, doi: 10.1016/j.chemosphere.2021.131344.

[5] V. H. Nguyen *et al.*, "Photocatalytic NOx abatement: Recent advances and emerging trends in the development of photocatalysts," *J. Clean. Prod.*, vol. 270, no. x, p. 121912, 2020, doi: 10.1016/j.jclepro.2020.121912.

[6] T. H. Panigrahi, S. R. Sahoo, G. Murmu, D. Maity, and S. Saha, "Current challenges and developments of inorganic/organic materials for the abatement of toxic nitrogen oxides (NOx) – A critical review," *Prog. Solid State Chem.*, vol. 68, no. 2, p. 100380, 2022, doi: 10.1016/j.progsolidstchem.2022.100380.

[7] A. Talaiekhozani, S. Rezania, K. H. Kim, R. Sanaye, and A. M. Amani, "Recent advances in photocatalytic

removal of organic and inorganic pollutants in air," *J. Clean. Prod.*, vol. 278, p. 123895, 2021, doi: 10.1016/j.jclepro.2020.123895.

[8] M. S. S. Danish *et al.*, "Photocatalytic applications of metal oxides for sustainable environmental remediation," *Metals (Basel).*, vol. 11, no. 1, pp. 1–25, 2021, doi: 10.3390/met11010080.

[9] C. Sun, J. A. Alonso, and J. Bian, "Recent Advances in Perovskite-Type Oxides for Energy Conversion and Storage Applications," *Adv. Energy Mater.*, vol. 11, no. 2, pp. 1–21, 2021, doi: 10.1002/aenm.202000459.

[10] R. Djellabi, M. F. Ordonez, F. Conte, E. Falletta, C. L. Bianchi, and I. Rossetti, "A review of advances in multifunctional XTiO3 perovskite-type oxides as piezo-photocatalysts for environmental remediation and energy production," *J. Hazard. Mater.*, vol. 421, no. May 2021, p. 126792, 2022, doi: 10.1016/j.jhazmat.2021.126792.

[11] R. Sasikala *et al.*, "Strontium titanate perovskite embedded reduced graphene oxide photoanode for dye-sensitized solar cell," *Opt. Mater. (Amst).*, vol. 136, no. January, p. 113464, 2023, doi: 10.1016/j.optmat.2023.113464.

[12] B. L. Phoon, C. W. Lai, J. C. Juan, P. L. Show, and G. T. Pan, "Recent developments of strontium titanate for photocatalytic water splitting application," *Int. J. Hydrogen Energy*, vol. 44, no. 28, pp. 14316–14340, 2019, doi: 10.1016/j.ijhydene.2019.01.166.

[13] C. H. A. Tsang *et al.*, "Titanium oxide based photocatalytic materials development and their role of in the air pollutants degradation: Overview and forecast," *Environ. Int.*, vol. 125, no. January, pp. 200–228, 2019, doi: 10.1016/j.envint.2019.01.015.

[14] R. Marschall, "Semiconductor composites: Strategies for enhancing charge carrier separation to improve photocatalytic activity," *Adv. Funct. Mater.*, vol. 24, no. 17, pp. 2421–2440, 2014, doi: 10.1002/adfm.201303214.

[15] J. P. Jeon, D. H. Kweon, B. J. Jang, M. J. Ju, and J. B. Baek, "Enhancing the Photocatalytic Activity of TiO2 Catalysts," *Adv. Sustain. Syst.*, vol. 4, no. 12, pp. 1–19, 2020, doi: 10.1002/adsu.202000197.

[16] Z. Chen, H. Yin, R. Wang, Y. Peng, C. You, and J. Li, "Efficient Electron Transfer by Plasmonic Silver in SrTiO3

for Low-Concentration Photocatalytic NO Oxidation," *Environ. Sci. Technol.*, vol. 56, no. 6, pp. 3604–3612, 2022.

[17] N. Zhou, V. López-Puente, Q. Wang, L. Polavarapu, I. Pastoriza-Santos, and Q. H. Xu, "Plasmon-enhanced light harvesting: Applications in enhanced photocatalysis, photodynamic therapy and photovoltaics," *RSC Advances*, vol. 5, no. 37. pp. 29076–29097, 2015, doi: 10.1039/c5ra01819f.

[18] X. Zhang, Y. L. Chen, R.-S. Liu, and D. P. Tsai, "Plasmonic photocatalysis," *Reports Prog. Phys.*, vol. 76, no. 4, p. 046401, Apr. 2013, doi: 10.1088/0034-4885/76/4/046401.

[19] Q. Zhang, Y. Huang, L. Xu, J. J. Cao, W. Ho, and S. C. Lee, "Visible-Light-Active Plasmonic Ag-SrTiO3 Nanocomposites for the Degradation of NO in Air with High Selectivity," *ACS Appl. Mater. Interfaces*, vol. 8, no. 6, pp. 4165–4174, 2016, doi: 10.1021/acsami.5b11887.

[20] L. A. Navarro, X. Perpiñà, M. Vellvehi, D. Sánchez, and X. Jordà, "Sintering Process Analysis for Die-Attach of Power Packages for High Temperature Applications based on Silver Nano-Particles Sintering Process Analysis for Die - Attach of Power Packages for High Temperature Applications based on Silver Nano - Particles," no. September, 2014.

[21] A. Fakharzadeh, R. Ebrahimi-Kahrizsangi, B. Nasiri-Tabrizi, and W. Jefrey Basirun, "Effect of dopant loading on the structural features of silver-doped hydroxyapatite obtained by mechanochemical method," *Ceram. Int.*, vol. 43, no. 15, pp. 12588–12598, 2017, doi: 10.1016/j.ceramint.2017.06.136.

[22] M. Stucchi, D. Meroni, G. Safran, A. Villa, C. L. Bianchi, and L. Prati, "Noble Metal Promoted TiO2 from Silver-Waste Valorisation: Synergism between Ag and Au," *Catalysts*, vol. 12, no. 2, pp. 1–17, 2022, doi: 10.3390/catal12020235.

[23] L. Fabbrini *et al.*, "Sr1-xAgxTiO3±δ (x = 0, 0.1) perovskite-structured catalysts for the flameless combustion of methane," *J. Catal.*, vol. 232, no. 2, pp. 247–256, 2005, doi: 10.1016/j.jcat.2005.03.012.

[24] M. Mori, M. Shibata, E. Kyuno, and S. Ito, "Reaction of hydrogen peroxide with titanium (IV) at different pH values," *Bull. Chem. Soc. Jpn.*, vol. 29, no. 8, pp. 904–907, 1956.

[25] B. Yin, H. Ma, S. Wang, and S. Chen, "Electrochemical synthesis of silver nanoparticles under protection of

poly(N-vinylpyrrolidone)," *J. Phys. Chem. B*, vol. 107, no. 34, pp. 8898–8904, 2003, doi: 10.1021/jp0349031.

[26] G. Dong, L. Yang, F. Wang, L. Zang, and C. Wang, "Removal of nitric oxide through visible light photocatalysis by g-C3N4 modified with perylene imides," *ACS Catal.*, vol. 6, no. 10, pp. 6511–6519, 2016.

[27] Q. Zhang *et al.*, "Perovskite LaFeO3-SrTiO3 composite for synergistically enhanced NO removal under visible light excitation," *Appl. Catal. B Environ.*, vol. 204, pp. 346–357, 2017.

[28] S. Jin, G. Dong, J. Luo, F. Ma, and C. Wang, "Improved photocatalytic NO removal activity of SrTiO3 by using SrCO3 as a new co-catalyst," *Appl. Catal. B Environ.*, vol. 227, pp. 24–34, 2018.

[29] J. Xiao *et al.*, "Simultaneously Tuning the Defects and Surface Properties of Ta3N5Nanoparticles by Mg-Zr Codoping for Significantly Accelerated Photocatalytic H2Evolution," *J. Am. Chem. Soc.*, vol. 143, no. 27, pp. 10059–10064, 2021, doi: 10.1021/jacs.1c04861.

[30] X. Guan, S. Zong, L. Tian, and M. Liu, "Efficient photocatalytic hydrogen production under visible-light irradiation on SrTiO3 without noble metal: dye-sensitization and earth-abundant cocatalyst modification," *Mater. Today Chem.*, vol. 26, p. 101018, 2022, doi: 10.1016/j.mtchem.2022.101018.

[31] S. Tonda, S. Kumar, O. Anjaneyulu, and V. Shanker, "Synthesis of Cr and La-codoped SrTiO3 nanoparticles for enhanced photocatalytic performance under sunlight irradiation," *Phys. Chem. Chem. Phys.*, vol. 16, no. 43, pp. 23819–23828, 2014, doi: 10.1039/c4cp02963a.

[32] A. S. Al-Fatesh *et al.*, "Effect of pre-treatment and calcination temperature on Al2O3-ZrO2 supported Ni-Co catalysts for dry reforming of methane," *Int. J. Hydrogen Energy*, vol. 44, no. 39, pp. 21546–21558, 2019, doi: 10.1016/j.ijhydene.2019.06.085.

[33] S. Adhami *et al.*, "Influence of the specific surface area and silver crystallite size of mesoporous Ag/SrTiO3 on the selectivity enhancement of ethylene oxide production," *J. Chem. Technol. Biotechnol.*, vol. 94, no. 12, pp. 3839–3849, 2019, doi: 10.1002/jctb.6182.

[34] P. Makuła, M. Pacia, and W. Macyk, "How To Correctly Determine the Band Gap Energy of Modified Semiconductor Photocatalysts Based on UV-Vis Spectra," *J. Phys. Chem. Lett.*, vol. 9, no. 23, pp. 6814–6817, 2018,

doi: 10.1021/acs.jpclett.8b02892.

[35] S. Landi, I. R. Segundo, E. Freitas, M. Vasilevskiy, J. Carneiro, and C. J. Tavares, "Use and misuse of the Kubelka-Munk function to obtain the band gap energy from diffuse reflectance measurements," *Solid State Commun.*, vol. 341, no. July 2021, pp. 1–7, 2022, doi: 10.1016/j.ssc.2021.114573.

[36] K. S. Kiran, B. S. Ashwath Narayana, and S. V Lokesh, "Enhanced photocatalytic activity of perovskite SrTiO3 nanorods," *Solid State Technol*, vol. 63, no. 4, pp. 1913–1920, 2020.

[37] U. Sulaeman, S. Yin, and T. Sato, "Solvothermal synthesis and photocatalytic properties of chromium-doped SrTiO3 nanoparticles," *Appl. Catal. B Environ.*, vol. 105, no. 1–2, pp. 206–210, 2011, doi: 10.1016/j.apcatb.2011.04.017.

[38] T. S. Jamil, H. A. Abbas, A. M. Youssief, E. S. Mansor, and F. F. Hammad, "The synthesis of nano-sized undoped, Bi doped and Bi, Cu co-doped SrTiO3 using two sol–gel methods to enhance the photocatalytic performance for the degradation of dibutyl phthalate under visible light," *Comptes Rendus Chim.*, vol. 20, no. 2, pp. 97–106, 2017, doi: 10.1016/j.crci.2016.05.022.

[39] L. F. Da Silva *et al.*, "An Understanding of the Photocatalytic Properties and Pollutant Degradation Mechanism of SrTiO3 Nanoparticles," *Photochem. Photobiol.*, vol. 92, no. 3, pp. 371–378, 2016, doi: 10.1111/php.12586.

[40] J. Lefebvre, F. Galli, C. L. Bianchi, G. S. Patience, and D. C. Boffito, "Experimental methods in chemical engineering: X-ray photoelectron spectroscopy-XPS," *Can. J. Chem. Eng.*, vol. 97, no. 10, pp. 2588–2593, 2019, doi: 10.1002/cjce.23530.

[41] M. G. Galloni, G. Cerrato, A. Giordana, E. Falletta, and C. L. Bianchi, "Sustainable Solar Light Photodegradation of Diclofenac by Nano- and Micro-Sized SrTiO3," *Catalysts*, vol. 12, no. 8, 2022, doi: 10.3390/catal12080804.

[42] M. A. Kafeshani, V. Mahdikhah, and S. Sheibani, "Facile preparation and modification of SrTiO3 through Ni–Cd co-doping as an efficient visible-light-driven photocatalyst," *Opt. Mater. (Amst).*, vol. 133, no. September, p. 113080, 2022, doi: 10.1016/j.optmat.2022.113080.

[43] M. E. Pilleux, C. R. Grahmann, and V. M. Fuenzalida, "Hydrothermal Strontium Titanate Films on Titanium:

An XPS and AES Depth-Profiling Study," *J. Am. Ceram. Soc.*, vol. 77, no. 6, pp. 1601–1604, 1994, doi: 10.1111/j.1151-2916.1994.tb09763.x.

[44] U. Diebold and T. E. Madey, "TiO2 by XPS," *Surf. Sci. Spectra*, vol. 4, no. 3, pp. 227–231, 1996.

[45] O. Schalm *et al.*, "A dataset of high-resolution synchrotron x-ray photoelectron spectra of tarnished silver-copper surfaces before and after reduction with a remote helium plasma at atmospheric pressure," *Data Br.*, vol. 35, p. 106872, 2021, doi: 10.1016/j.dib.2021.106872.

[46] S. W. Lee, S. Obregón, and V. Rodríguez-González, "The role of silver nanoparticles functionalized on TiO2 for photocatalytic disinfection of harmful algae," *RSC Adv.*, vol. 5, no. 55, pp. 44470–44475, 2015, doi: 10.1039/c5ra08313c.

[47] A. Bedon and A. Glisenti, "Chapter Developing Functionality in Perovskites from Abatement of Pollutants to Sustainable Energy Conversion and Storage," 2020.

[48] J. Xie *et al.*, "Enhancing H2 Evolution by Adjusting Oxygen Species at Perovskite SrTiO3," *ACS Appl. Energy Mater.*, vol. 5, no. 8, pp. 9559–9570, 2022.

[49] J. Wang, H. Li, H. Li, S. Yin, and T. Sato, "Preparation and photocatalytic activity of visible light-active sulfur and nitrogen co-doped SrTiO3," *Solid State Sci.*, vol. 11, no. 1, pp. 182–188, 2009, doi: 10.1016/j.solidstatesciences.2008.04.010.

[50] T. Ohno, T. Tsubota, Y. Nakamura, and K. Sayama, "Preparation of S, C cation-codoped SrTiO3 and its photocatalytic activity under visible light," *Appl. Catal. A Gen.*, vol. 288, no. 1–2, pp. 74–79, 2005, doi: 10.1016/j.apcata.2005.04.035.

[51] Y. Wu *et al.*, "Solvothermal fabrication of La-WO3/SrTiO3 heterojunction with high photocatalytic performance under visible light irradiation," *Sol. Energy Mater. Sol. Cells*, vol. 176, pp. 230–238, 2018.

[52] S. Wan, M. Chen, M. Ou, and Q. Zhong, "Plasmonic Ag nanoparticles decorated SrTiO3 nanocubes for enhanced photocatalytic CO2 reduction and H2 evolution under visible light irradiation," *J. CO2 Util.*, vol. 33, pp. 357–364, 2019.

[53] X. Guan and L. Guo, "Cocatalytic effect of SrTiO3 on Ag3PO4 toward enhanced photocatalytic water oxidation," *Acs Catal.*, vol. 4, no. 9, pp. 3020–3026, 2014.

[54] H. A. Rafaie, R. M. Nor, M. S. Azmina, N. I. T. Ramli, and R. Mohamed, "Decoration of ZnO microstructures with Ag nanoparticles enhanced the catalytic photodegradation of methylene blue dye," *J. Environ. Chem. Eng.*, vol. 5, no. 4, pp. 3963–3972, 2017, doi: 10.1016/j.jece.2017.07.070.

[55] S. Jin, G. Dong, J. Luo, F. Ma, and C. Wang, "Improved photocatalytic NO removal activity of SrTiO3 by using SrCO3 as a new co-catalyst," *Appl. Catal. B Environ.*, vol. 227, no. October 2017, pp. 24–34, 2018, doi: 10.1016/j.apcatb.2018.01.020.

[56] Y. Cui *et al.*, "Enhanced solar photocatalytic degradation of nitric oxide using graphene quantum dots/bismuth tungstate composite catalysts," *Chem. Eng. J.*, vol. 420, no. P1, p. 129595, 2021, doi: 10.1016/j.cej.2021.129595.

[57] H. Dong, J. Sun, G. Chen, C. Li, Y. Hu, and C. Lv, "An advanced Ag-based photocatalyst Ag2Ta4O11 with outstanding activity, durability and universality for removing organic dyes," *Phys. Chem. Chem. Phys.*, vol. 16, no. 43, pp. 23915–23921, 2014, doi: 10.1039/c4cp03494e.

[58] H. Bentour, M. El Yadari, A. El Kenz, and A. Benyoussef, "DFT study of electronic and optical properties of (S–Mn) co-doped SrTiO3 for enhanced photocatalytic hydrogen production," *Solid State Commun.*, vol. 312, no. February, 2020, doi: 10.1016/j.ssc.2020.113893.

[59] V. Lalan, V. P. Mahadevan Pillai, and K. G. Gopchandran, "Enhanced electron transfer due to rGO makes Ag–CaTiO3@rGO a promising plasmonic photocatalyst," *J. Sci. Adv. Mater. Devices*, vol. 7, no. 3, p. 100468, 2022, doi: 10.1016/j.jsamd.2022.100468.

[60] Z. H. Shah, Y. Ge, W. Ye, X. J. Lin, S. Zhang, and R. Lu, "Visible light activation of SrTiO3 by loading Ag/AgX (X = Cl, Br) for highly efficient plasmon-enhanced photocatalysis," *Mater. Chem. Phys.*, vol. 198, pp. 73–82, 2017, doi: 10.1016/j.matchemphys.2017.05.002.